

Emission line profiles from self-gravitating toroids around black holes

Fumihiko Usui¹, Shogo Nishida² and Yoshiharu Eriguchi²

¹*Department of Earth Science and Astronomy, College of Arts and Sciences, University of Tokyo, Meguro, Tokyo 153, Japan*

²*Department of Earth Science and Astronomy, Graduate School of Arts and Sciences, University of Tokyo, Meguro, Tokyo 153, Japan*

Updated 25 September 2018

ABSTRACT

We have computed line profiles from self-gravitating toroids around black holes. The specific angular momentum of the toroids is assumed to be constant in space. The images of the toroids show peculiar feature in the rear side of the black holes. Concerning the line profiles, the red wing extends to the very small frequency region because the location of the inner edge is rather near the event horizon of the black hole and consequently the velocity of the inner edge of toroids can be faster than that of the Kepler disks.

Key words: Black holes – Accretion disks – Self-gravitating toroids – Emission Line profiles

1 INTRODUCTION

Recently, strong evidence for existence of supermassive black holes in the central regions of galaxies has been found from observations of electromagnetic waves with various wavelengths ranging from the radio waves to X-rays (see e.g. Miyoshi et al. 1995 for the radio observation; Ford et al. 1994, Harms et al. 1994 for the optical observation; Tanaka et al. 1995 for the X-ray observation). Radio and optical observations have shown that there exist very rapidly rotating gaseous disks in the central regions of galaxies. Since the high velocity of a disk implies the existence of a large amount of mass within a region of a very small size, it is widely considered that there are supermassive black holes with masses of $10^7 \sim 10^9 M_{\odot}$ at the centers of galaxies. However, such observations do not reveal the nature of black holes because the size of the observed region is still too large to get detailed information about the black holes.

Contrary to these optical and radio analyses, recent X-ray observations have brought us important information about gravitational fields very near the massive objects or black holes. By using the ASCA satellite, broad iron emission lines have been detected in active galaxies (see e.g. Fabian et al. 1994; Mushotzky et al. 1995). In particular, Tanaka et al. (1995) observed the Seyfert 1 galaxy, MCG–6–30–15, and discovered a very broad and skewed iron emission line. The broadness and skewness of the line profile can be explained only by assuming that the inner edge of the accretion disk is located very near the event horizon of the

central black hole (Tanaka et al. 1995; Fabian et al. 1995). It implies that X-ray observations can be used to understand the very vicinity of the black holes. It is important to know the gravitational field near the event horizon because it is the key feature to distinguish a Schwarzschild black hole from a Kerr black hole.

Consequently we have reached a stage to investigate very strong gravitational fields of black holes and to be able to test the validity of general relativity. However, since the emission line profiles depend not only on the gravitational fields but also on the structures of the accretion disks, it is not easy to determine the type of the black hole, i.e. whether the central black hole is of a Schwarzschild type or of a Kerr type. In fact, concerning the nature of the black hole at the center of MCG–6–30–15, various discussions have not settled down to a unique interpretation yet (see e.g. Tanaka et al. 1995; Iwasawa et al. 1996; Dabrowski et al. 1997; Bromley et al. 1997; Reynolds & Begelman 1997; Bromley et al. 1998). Therefore, in order to get a consistent picture of black hole – accretion disk systems, we have to pursue much more investigations theoretically as well as observationally.

Concerning the theory about the spectra of accretion disks, Cunningham (1975) was the first to formulate the problem for Kerr black holes and obtained theoretical spectra from accretion disks around black holes (see also Cunningham 1976). Gerbal & Pelat (1981) investigated lines from a ring around a black hole and found double-peaked asymmetric profiles. From the end of 80's, observations of lines in the X-ray spectrum stimulated many authors to

study line profiles of accretion disks as well as disk structures (e.g. Nandra et al. 1989; Fabian et al. 1989; Kunieda et al. 1990; Kojima 1991; Laor 1991; Chen & Halpern 1989, 1990). However, in almost all theoretical studies mentioned above, investigations of the emission line profiles have been done by assuming that disks are geometrically thin and that only direct photons are observed.

Some authors have studied the effect of multiple images (Luminet 1978; Bao, Hadrava & Østgaard 1994) and that of self-eclipse due to toroidal configurations (Bao & Stuchlik 1992; Kojima & Fukue 1992). For toroidal configurations the rotation law of the toroid is not always that of the Kepler rotation because of the presence of the pressure within the toroid. In fact, Kojima & Fukue (1992) employed a variety of rotation laws. However, their analysis was done in the framework of Newtonian gravity. Therefore, quantitative treatment of non-Keplerian toroids in general relativity has not been carried out yet.

Furthermore, in some situations, self-gravity of disks or toroids plays an important role for the structures of disks or toroids. In particular, massive neutron toroids around neutron stars or black holes have been proposed as possible sources of γ -ray bursts (e.g. Paczyński 1991; Narayan, Paczyński & Piran 1992; Jaroszyński 1993; Witt et al. 1994). Although there might be little chance to observe line profiles from such systems even if exist, it would be interesting to study the effect of self-gravity of toroids on the line profiles. Such self-gravitating disks were investigated by Karas, Lanza & Vokrouhlicky (1995). However, they have studied very light thin disks whose mass is less than several percent of the mass of the black hole. From the theoretical point of view, it would be interesting to investigate more massive disks or toroids as well as the effect of geometrical thickness. By treating massive toroids, the central objects are no more of Schwarzschild type nor Kerr type black holes because of the gravitational effect of the self-gravitating massive toroids on the black holes (Nishida & Eriguchi 1994). Moreover, gravitational effect of massive toroids may bring some differences to line profiles. Therefore, in this paper, we will consider self-gravitating toroid – black hole systems and study their effect on emission line profiles.

2 METHOD OF CALCULATION

2.1 Toroid – black hole systems

We will solve the spacetime around a self-gravitating and geometrically thick toroid – black hole system and study photon trajectories emitted from the toroid. The setting of the system is shown in Fig. 1. The black hole is located at the origin of the coordinate system and the equatorial plane of the accretion toroid coincides with the X - Y plane. Distances from the black hole to the inner and outer edges of the toroid are r_{in} and r_{out} , respectively. The position of an observer is assumed to be at $r = r_{\text{obs}}$ and $\theta = \theta_0$ in the Y - Z plane. Here (r, θ, φ) are the spherical coordinates.

In order to obtain data for the images of the toroid and the line profiles, we consider a screen perpendicular to the line connecting the black hole and the observer. A set of intersections of tangential lines to the photon trajectories with this screen forms an image of the toroid. On this screen,

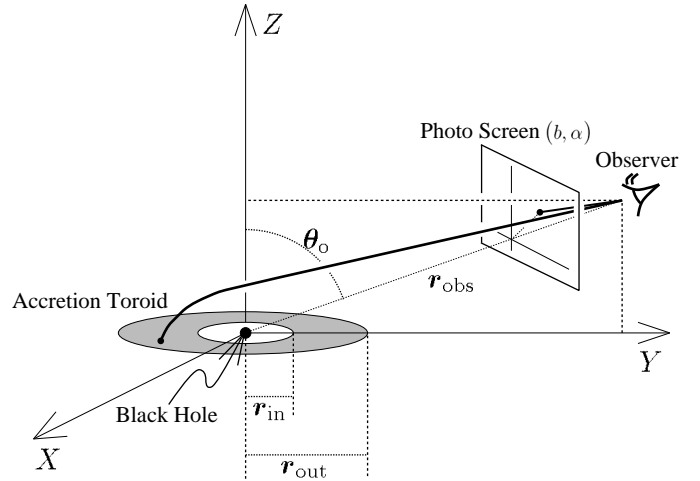


Figure 1. Schematic view of the toroid – black hole system. The observer is located at $(r_{\text{obs}}, \theta_0)$. The coordinates of the intersection of the tangential line to the photon trajectory with the screen are expressed as $(b \cos \alpha, b \sin \alpha)$. The distances to the inner and outer edges of the toroid from the black hole are r_{in} and r_{out} , respectively.

we set the polar coordinates (b, α) whose origin is at the intersection of the line connecting the black hole and the observer with the screen.

2.2 Metric and photon trajectories

Since we will treat *stationary* and *axisymmetric* toroid – black hole systems, the line element can be written in the pseudo-isotropic coordinates as follows:

$$ds^2 = -e^{2\psi} dt^2 + e^{2\xi} \left(\frac{1}{1 - 2M/r + J^2/(Mr)^2} dr^2 + r^2 d\theta^2 \right) + e^{2\zeta} r^2 \sin^2 \theta (d\phi - \omega dt)^2, \quad (1)$$

where t and ϕ are the coordinates associated with time and axial Killing vectors, respectively and M and J are the gravitational mass and the total angular momentum of the black hole, respectively. Metric components ψ , ξ , ζ and ω are functions of r and θ . This metric reduces to that of the Schwarzschild coordinates in the spherical limit. Hereafter we use the units of $c = G = 1$.

We employ the numerical code of Nishida & Eriguchi (1994) to solve the structures of toroids and the metric functions. The matter of the toroid is assumed to be polytrope as follows:

$$p = K\rho^{1+1/N}, \quad \varepsilon = \rho + Np, \quad (2)$$

where p , ρ , ε , N and K are the pressure, the rest mass density, the energy density, the polytropic index and a constant, respectively. We choose $N = 3$ polytropes in this paper. Concerning the rotation law of the toroid, the specific angular momentum l is assumed to be constant, i.e. $l = \text{constant}$.

Trajectories of photons emitted from the surface of the toroid are followed up to the observer. This can be done by integrating the geodesic equation for photons:

$$\frac{du^\alpha}{d\lambda} + \Gamma_{\mu\nu}^\alpha u^\mu u^\nu = 0, \quad (3)$$

where λ is an Affine parameter, u^α is the four-velocity of the photon which is defined by

$$u^\alpha = \frac{dx^\alpha}{d\lambda}, \quad (4)$$

and $\Gamma_{\mu\nu}^\alpha$ is the Christoffel symbol.

Although photons are emitted from the surface of the toroid, we integrate the geodesic equation starting from the observer position back to the toroid. If the geodesic hits the surface of the toroid, we can get one trajectory of a photon connecting the surface of the toroid and the observer. Thus the geodesic equation is integrated by choosing initial values for the four-velocity at the observer position. Since the metric functions are solved on discrete mesh points, we need to interpolate the metric functions at points where the geodesic passes. Once a geodesic curve from the toroid to the observer is obtained, the position of the image on the screen can be determined. By integrating many photon trajectories, we have an image of the toroid on the screen and investigate the spectrum from the toroid. In practice, we have computed (100×100) photon trajectories by choosing initial velocities so that tangential lines hit mesh points on the screen which are equidistantly distributed.

2.3 Observed total intensity

In order to calculate the observed total intensity from the toroid, we need to specify the distribution of emissivity of the toroid. For geometrically thin and nonself-gravitating disks, there are several models for emissivity (e.g. Novikov & Thorne 1973; Page & Thorne 1974), but they are not decisive ones because of the lack of observational data. The situation is worse for self-gravitating toroids. Therefore, at the present stage, we adopt a simplified model in which the emissivity is assumed to be a power of the distance from the rotation axis as follows:

$$e = kR^s, \quad (5)$$

where e , k and s are the emissivity and two constants, respectively, and R is the distance from the rotation axis defined as

$$R = r \sin \theta. \quad (6)$$

Since the toroid is rotating around the black hole, the energy of photons emitted from the toroid is shifted due to the Doppler effect and the gravitational redshift by the following factor g :

$$g \equiv \frac{1}{1+z} = \frac{E_{\text{obs}}}{E_{\text{em}}}, \quad (7)$$

where z , E_{em} and E_{obs} are the redshift, the energy of the emitted photon and the energy of the observed photon, respectively. Since the matter in the toroid is assumed to move only in the azimuthal direction, the energy of the emitted photon is expressed as

$$E_{\text{em}} = p_t u^t + p_\phi u^\phi = p_t u^t \left(1 + \Omega_t \frac{p_\phi}{p_t} \right), \quad (8)$$

where u^t , u^ϕ , p_t and p_ϕ are the t - and ϕ -components of the four-velocity of the toroid and the covariant t - and ϕ -

components of the four-momentum of the photon, respectively. The quantity Ω_t is the angular velocity of the toroid which is defined as

$$\Omega_t = \frac{u^\phi}{u^t}. \quad (9)$$

This angular velocity can be expressed as follows for the constant specific angular momentum toroid:

$$\Omega_t = \omega + \frac{l}{(e^{\zeta-\psi} r \sin \theta)^2 (1-l\omega)}. \quad (10)$$

The component u^t can be calculated from the normalization condition $u_\mu u^\mu = -1$ as follows:

$$u^t = \frac{1}{\sqrt{e^{2\psi} - e^{2\zeta} r^2 \sin^2 \theta (\Omega_t - \omega)^2}}. \quad (11)$$

Since photons travel in the axisymmetric and stationary spacetime, quantities p_t and p_ϕ are conserved along the photon trajectories. Thus, the energy of the observed photon is given as $E_{\text{obs}} = p_t$ and the ratio $1+z = E_{\text{em}}/E_{\text{obs}}$ can be expressed as follows:

$$1+z = u^t \left(1 + \Omega_t \frac{p_\phi}{p_t} \right). \quad (12)$$

In this equation, the quantity p_ϕ/p_t is the impact parameter of the photon around the Z -axis and is expressed as

$$p_\phi/p_t = b \sin \theta_0 \sin \alpha. \quad (13)$$

By using this redshift factor, the observed total intensity $I_{\text{obs}}^{(0)}$ can be calculated from the intrinsic total intensity of the source $I_{\text{em}}^{(0)}$ as follows:

$$I_{\text{obs}}^{(0)} = \left(\frac{1}{1+z} \right)^4 I_{\text{em}}^{(0)}. \quad (14)$$

The 4th power in this expression may be understood as (1) the Doppler effect by the rotation of the toroid (one power), (2) the redshift by the gravitational field (one power), and (3) the focusing effect by the gravitational lens effect (two power) (see e.g. Luminet 1978).

2.4 Line profiles

The observed specific flux $dF_{\text{obs}}(E_{\text{obs}})$ within the solid angle $d\Omega$ can be calculated from

$$dF_{\text{obs}}(E_{\text{obs}}) = I_{\text{obs}}(E_{\text{obs}}) d\Omega = g^3 I_{\text{em}}(E_{\text{em}}) d\Omega, \quad (15)$$

where I_{obs} and I_{em} are the observed specific intensity and the specific intensity at the source, respectively. In this equation we have made use of the invariance of the quantity I/E^3 along the geodesics. Since we consider a narrow line, the specific intensity I_{em} in the rest frame of the source is assumed to be a delta function as follows:

$$I_{\text{em}}(E_{\text{em}}) = e(R) \delta(E_{\text{em}} - E_0), \quad (16)$$

where e is the emissivity given in equation (5) and E_0 is the rest energy of the emitted photon. In this paper, the emission is assumed to be isotropic.

3 NUMERICAL RESULTS

3.1 Models for toroid – black hole systems

We have computed three equilibrium configurations of toroid – black hole systems and their metric components by using the general relativistic code (Nishida & Eriguchi 1994): models with the mass ratio $q \equiv m/M = 0.012$ (Model A hereafter), 0.080 (Model B) and 0.49 (Model C) where m is the mass of the toroid. As mentioned in Introduction, it should be noted that the central object is neither a Schwarzschild nor a Kerr black hole because of *deformation* due to gravity of the toroid. It implies that the spacetime is different from that of Schwarzschild or Kerr. Parameters of the models are shown in Table 1. In this Table, ε_0 , ω_H and r_H are the maximum energy density of the toroid, the value of the potential ω on the event horizon and the horizon radius, respectively. In order to compare our models with those of Kerr black holes, the values of J/M^2 and the ratios of the radius of the marginally stable orbit to the horizon radius are tabulated in Table 2. Here R_{ms} is the radius of the marginally stable orbit.

3.2 Images of toroids

Images of thin disks have been computed by several authors (e.g. Luminet 1978; Fukue & Yokoyama 1988; Fanton et al. 1997). The characteristic feature of images of thin disks is significant deformation of disk shapes in the rear of black holes. Similar deformation can be seen even for self-gravitating thick toroids (see Figure 2).

In this figure, images of self-gravitating toroids seen from different inclination angles are shown. The observer is assumed to be at $r_{\text{obs}} = 10.5r_H$. This distance has been chosen because the numerically solved spacetime covers only the region with $r \leq 2r_{\text{out}}$. Although it seems too near to the black hole, photon trajectories beyond this distance are almost straight so that the images of the toroids and the line profiles would be affected only little even if the observer is located at a more distant position.

Since the direction of the rotation of the toroid is counter-clockwise, the left part of the toroid is rotating toward the observer. In these pictures, the index of the emissivity is fixed to $s = -1$ and Model B is chosen, i.e. $q = 0.08$. The shape and the equi-energy density contours of the toroidal Model B in the meridional cross section are shown in Fig. 3.

The toroid with $\theta_0 = 5^\circ$ is observed almost from the direction of the rotation axis and shows almost a round disk shape. As the inclination angle is increased, the shape begins to be distorted by the gravitational lens effect. The front side of the toroid almost keeps its original shape, but the rear side is significantly warped. As for the thickness of the toroid, the image of the rear side of the toroid is narrower compared to that of the front side. One more significant feature is the appearance of an inner ring image inside the toroidal image. This ring image is one of the multiple images which are formed by photons orbiting several times around the black hole. In particular, this ring is formed by 2nd or higher order images because the 1st order image is hidden by the thickness of the toroid.

3.3 Line profiles from self-gravitating toroids

It is well known that the line profiles from disks or toroids around black holes show characteristic features as discussed in Introduction: 1) broad line profiles, in particular towards the red wing and 2) asymmetry of the line profiles. For thin disks, the profile varies as the inclination angle changes. When the inclination is small, $\theta_0 \lesssim 15^\circ$, the line profile has a single peak around the wavelength or the frequency shifted from the intrinsic value by the amount of the gravitational redshift and the wing extends more to the red side compared to the blue wing. As the inclination becomes large, $\theta_0 \gtrsim 15^\circ$, the peak shifts to the blue side because of the Doppler effect of the approaching region and the red wing extends further to the low frequency side also because of the Doppler shift of the receding inner region. At the same time, there appears a second peak in the red wing around the redshift factor which depends on the inclination angle and on the width of the disk. In other words, double-peaked feature, a strong blue peak and a weak red peak, appears. It is noted that positions of peaks are not affected by the types of the emissivity but depend on the inclination angle and on the width of thin disks. This is because the position of the peak is determined from the size of the area which has a same redshift factor on the surface of the toroid.

Concerning the self-gravitating toroids, the line profiles are shown in Figs. 4 and 5. In Fig. 4, the line profiles for Model B with $q = 0.08$ are displayed for four different emissivity indices $s = -1, -2, -3$ and -4 . As seen from these figures, although basic features of line profiles are similar to those of thin disks, double-peaked structures are no more pronounced even if they exist. This is mainly because a part of the surface of the toroid is eclipsed by the toroid itself (Kojima & Fukue 1992; Bao & Stuchlik 1992). However, this self-eclipse does not lead to flat-top profiles obtained by Kojima & Fukue (1992) because of the general relativistic effect.

It is remarkable that the value of g extends to 0.4 as seen from the profile for $\theta_0 = 60^\circ$. In order to get this value of the redshift for the Kepler disk around a Kerr black hole, the value of J/M^2 is 0.5 or so (see e.g. Dabrowski et al. 1997) and the inner edge of the disk must be located at the marginally stable orbit, i.e. $r_{\text{in}} = 2.27r_H$. On the contrary, for our toroidal model, those values are $J/M^2 = 0.706$ and $r_{\text{in}} = 1.27r_H$. This implies that the location of the inner edge can be much nearer to the central black hole for *toroidal* configurations compared to thin disk models in order to get models with the same value of the maximum redshift. This occurs because the rotation law is not Keplerian so that the inner edge of the toroid can be located nearer than the marginally stable radius for the Kepler disks. The similarity between our Model B and the Kerr black hole – Kepler disk model with $J/M^2 = 0.5$ can be seen in profiles for other moderate inclination angles apart from the blue side.

In Fig. 5, line profiles are shown for Models A–C with different inclination angles and the emissivity index $s = -1$. The effect of the toroidal gravity to the spacetime can be clearly seen by the shift of the line to the red side for profiles with smaller inclination angles because the redshift for these models is mainly due to gravity. For self-gravitating toroids, the energy is shifted significantly to the red side and the flux increases for every energy range. For Model C, we have

Table 1. Model parameters of toroid – black hole systems

Model	q	$J\varepsilon_0$	$M\varepsilon_0^{1/2}$	$\omega_H/\varepsilon_0^{1/2}$	J/M^2	r_{in}/r_H	r_{out}/r_H
A	1.2×10^{-2}	7.42×10^{-6}	6.23×10^{-3}	1.0×10^1	0.191	2.04	5.56
B	8.0×10^{-2}	3.86×10^{-4}	2.34×10^{-2}	1.0×10^1	0.706	1.37	4.59
C	4.9×10^{-1}	1.60×10^{-3}	4.61×10^{-2}	4.0	0.751	1.46	5.06

Table 2. Quantities for Kerr black holes

J/M^2	R_{ms}/r_H	Comment
0.0	3.00	Schwarzschild
0.191	2.71	J/M^2 is the same as Model A
0.50	2.27	
0.706	1.97	J/M^2 is the same as Model B
0.751	1.90	J/M^2 is the same as Model C
0.998	1.16	
1.00	1.00	Extreme Kerr

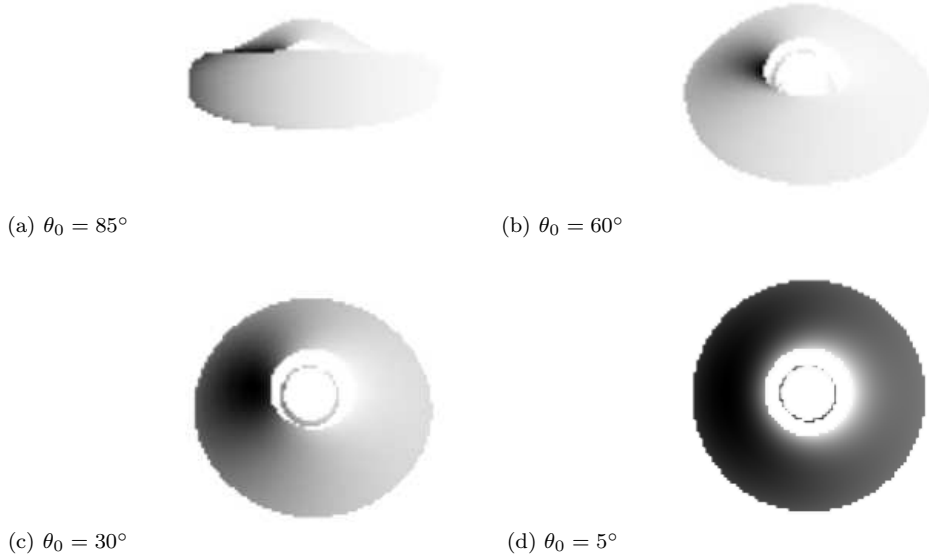


Figure 2. Images of the accretion toroidal Model B for different inclination angles θ_0 . The shade of this image indicates the distribution of the total surface brightness or the total intensity. For Model B the mass ratio and the emissivity index are $q = 0.08$ and $s = -1$, respectively. The inner radius $r_{\text{in}} = 1.37r_H$ and the outer radius $r_{\text{out}} = 4.59r_H$. The toroid rotates counter-clockwise so that the left part of the toroid is approaching the observer.

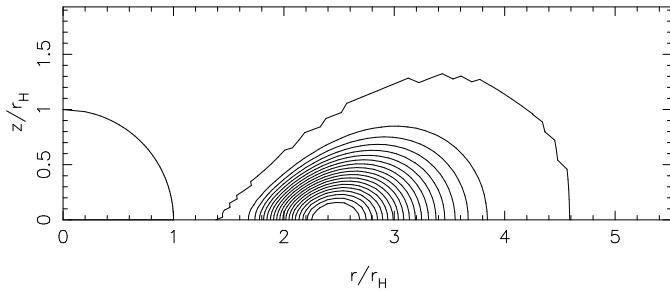


Figure 3. The contours of the energy density in a meridional cross section of Model B. The circle at the origin denotes the horizon of the black hole in this coordinates. The units of the distance is r_H .

obtained $g_{\min} = 0.2$ and $J/M^2 = 0.75$, where g_{\min} is the minimum value of the quantity g . In order to get $g_{\min} = 0.2$ for the Kerr model, we have to choose a nearly extreme Kerr black hole with $J/M^2 \sim 1.0$ (see e.g. Dabrowski et al. 1997). It should be noted that the inner edge of the toroid is located very near the central black hole, i.e. $r_{\text{in}} = 1.46r_{\text{H}}$ for our toroidal model and $r_{\text{in}} = 1.16r_{\text{H}}$ for the extreme Kerr case (see Table 2).

4 DISCUSSION AND CONCLUSION

In this paper we have constructed toroid – black hole systems in general relativity. We have computed photon trajectories in the numerically obtained gravitational fields and investigated the images of the toroids as well as the line profiles from the toroids. In these computations, we have assumed that the observer is located very near the black hole because the metric in the whole space has not been calculated. Therefore, the quantitative values in this paper will be changed a little if the observer is located at infinity. However, the important thing is not to obtain exact quantitative values but to know characteristic feature which appears only by introducing thickness and self-gravity numerically exactly. In this sense, our results serve as representative ones for self-gravitating toroids around black holes.

As discussed in Introduction, the observation of MCG–6–30–15 has given us time varying line profiles whose interpretation has not been clarified yet (Tanaka et al. 1995; Iwasawa et al. 1996; Dabrowski et al. 1997). Some authors have proposed models for the system which would explain the observations (Dabrowski et al. 1997; Bromley et al. 1997; Bromley et al. 1998). However, since there are many parameters about the disk structures and the X-ray sources, it is very difficult to obtain a unique solution for the system. This can be also seen from our result. For our Model B with the emissivity indices $s = -1$ and $s = -4$, the line profiles are shown in Fig. 6 together with the observational data. As seen from this figure, the tendency of the observational data seems to be roughly explained by the change of the emissivity index of Model B. Thus, at the present stage, we can only say that since the model cannot be uniquely determined, we have to get more accurate observational data to clarify the spacetime of the central region of galaxies.

ACKNOWLEDGMENT

We would like to thank Dr. A. Lanza for his discussion and his information about the paper in which self-gravitating thin disks are treated.

REFERENCES

Bao G., Stuchlik Z., 1992, ApJ, 400, 163
 Bao G., Hadrava P., Østgaard E., 1994, ApJ, 435, 55
 Bromley B.C., Chen K., Miller W.A., 1997, ApJ, 475, 57
 Bromley B.C., Miller W.A., Pariev V.I., 1998, Nat, 391, 54
 Chen K., Halpern J.P., 1989, ApJ, 344, 115
 Chen K., Halpern J.P., 1990, ApJ, 354, L1
 Cunningham C.T., 1975, ApJ, 202, 788
 Cunningham C.T., 1976, ApJ, 208, 534

Dabrowski Y., Fabian A.C., Iwasawa K., Lasenby A.N., Reynolds C.S., 1997, MNRAS, 288, L11
 Fabian A.C. et al., 1994, PASJ, 46, L59
 Fabian A.C., Nandra K., Reynolds C.S., Brandt W.N., Otani C., Tanaka Y., Inoue H., Iwasawa K., 1995, MNRAS, 277, L11
 Fabian A.C., Rees M.J., Stella L., White N.E., 1989, MNRAS, 238, 729
 Fanton C., Calvani M., de Felice F., Čadež A., 1997, PASJ, 49, 159
 Ford H.C., Harms R.J., Tsvetanov Z.I., Hartig G.F., Dressel L.L., Kriss G.A., Bohlin R.C., Davidsen A.F., Margon B., Kochhar A.K., 1994, ApJ, 435, L27
 Fukue J., Yokoyama T., 1988, PASJ, 40, 15
 Gerbal D., Pelat D., 1981, A&A, 95, 18
 Harms R.J., Ford H.C., Tsvetanov Z.I., Hartig G.F., Dressel L.L., Kriss G.A., Bohlin R.C., Davidsen A.F., Margon B., Kochhar A.K., 1994, ApJ, 435, L35
 Iwasawa K., Fabian A.C., Reynolds C.S., Nandra K., Otani C., Inoue H., Hayashida K., Brandt W.N., Dotani T., Kunieda H., Matsuoka M., Tanaka Y., 1996, MNRAS, 282, 1038
 Jaroszyński M., 1993, Acta Astronomica, 43, 183
 Karas V., Lanza A., Vokrouhlický D., 1995, ApJ, 440, 108
 Kojima Y., 1991, MNRAS, 250, 629
 Kojima Y., Fukue J., 1992, MNRAS, 256, 679
 Kunieda H., Turner M.J., Awaki H., Koyama K., Mushotzky R.F., Tsusaka Y., 1990, Nat, 345, 786
 Laor A., 1991, ApJ, 376, 90
 Luminet J.-P., 1978, A&A, 75, 228
 Miyoshi M., Moran J., Herrnstein J., Greenhill L., Nakai N., Diamond P., Inoue M., 1995, Nat, 373, 127
 Mushotzky R.F., Fabian A.C., Iwasawa K., Kunieda H., Matsuoka M., Nandra K., Tanaka Y., 1995, MNRAS, 272, L9
 Nandra K., Pounds K.A., Stewart G.C., Fabian A.C., Rees M.J., 1989, MNRAS, 236, 39p
 Narayan R., Paczyński B., Piran T., 1992, ApJ, 395, L83
 Nishida S., Eriguchi Y., 1994, ApJ, 427, 429
 Novikov I.D., Thorne K.S., 1973, in *Black Holes*, ed. C. DeWitt & B.S. DeWitt (New York; Gordon & Breach), p.343–450
 Paczyński B., 1991, Acta Astronomica, 41, 257
 Page D.N., Thorne K.S., 1974, ApJ, 191, 499
 Reynolds C.S., Begelman M.C., 1997, ApJ, 488, 109
 Tanaka Y., Nandra K., Fabian A.C., Inoue H., Otani C., Dotani T., Hayashida K., Iwasawa K., Kii T., Kunieda H., Makino F., Matsuoka M., 1995, Nat, 375, 659
 Witt H.J., Jaroszyński M., Haensel P., Paczyński B., Wambsgans J., 1994, ApJ, 422, 219

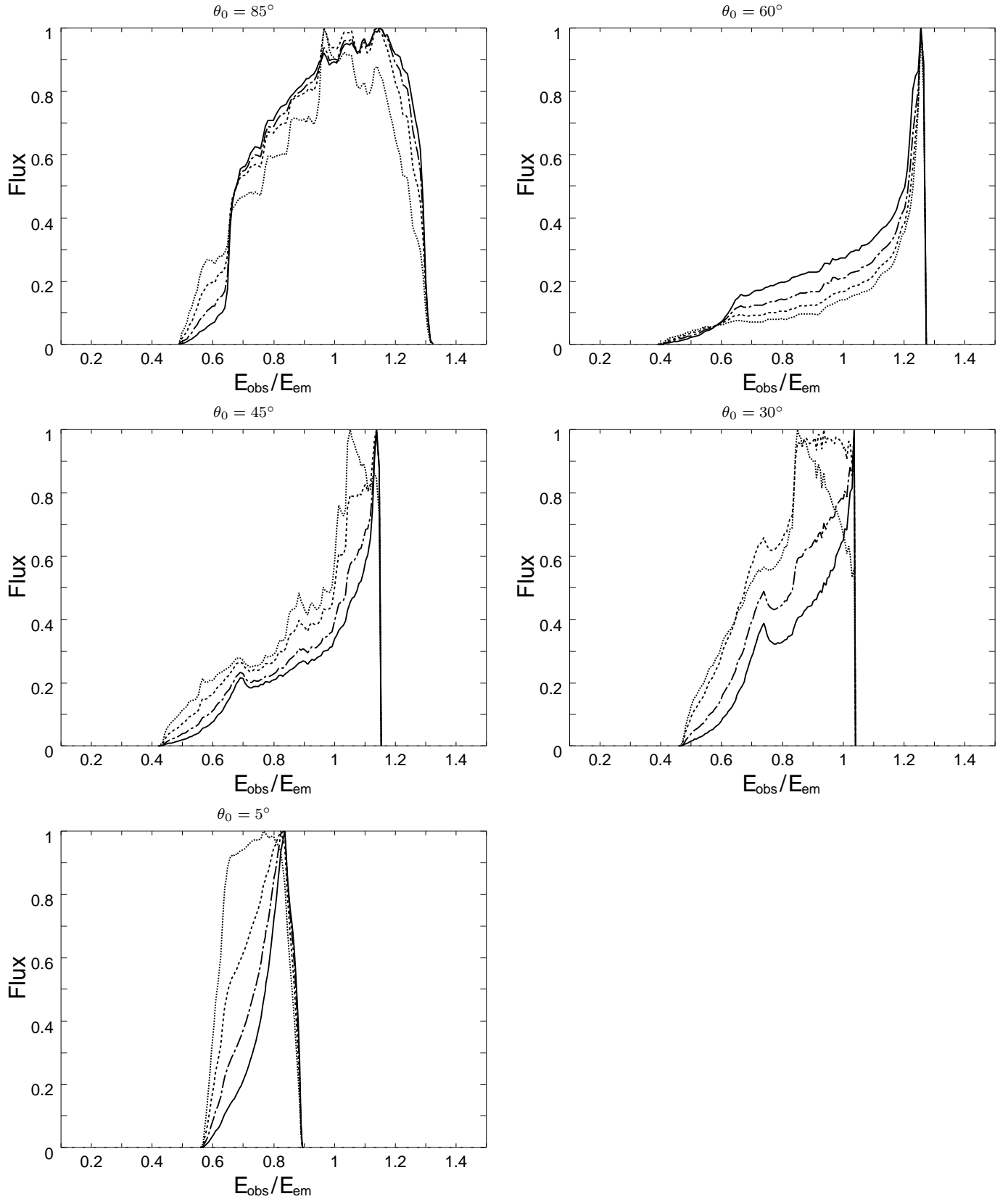


Figure 4. Line profiles of the accretion toroid (Model B, i.e. $q = 0.08$) are shown for different inclination angles θ_0 and for several emissivity indices s . Each flux is normalized so that its maximum becomes unity. The solid line, the dash-dotted line, the short dashed line and dotted line denote models with the emissivity indices $s = -1, -2, -3$ and -4 , respectively.

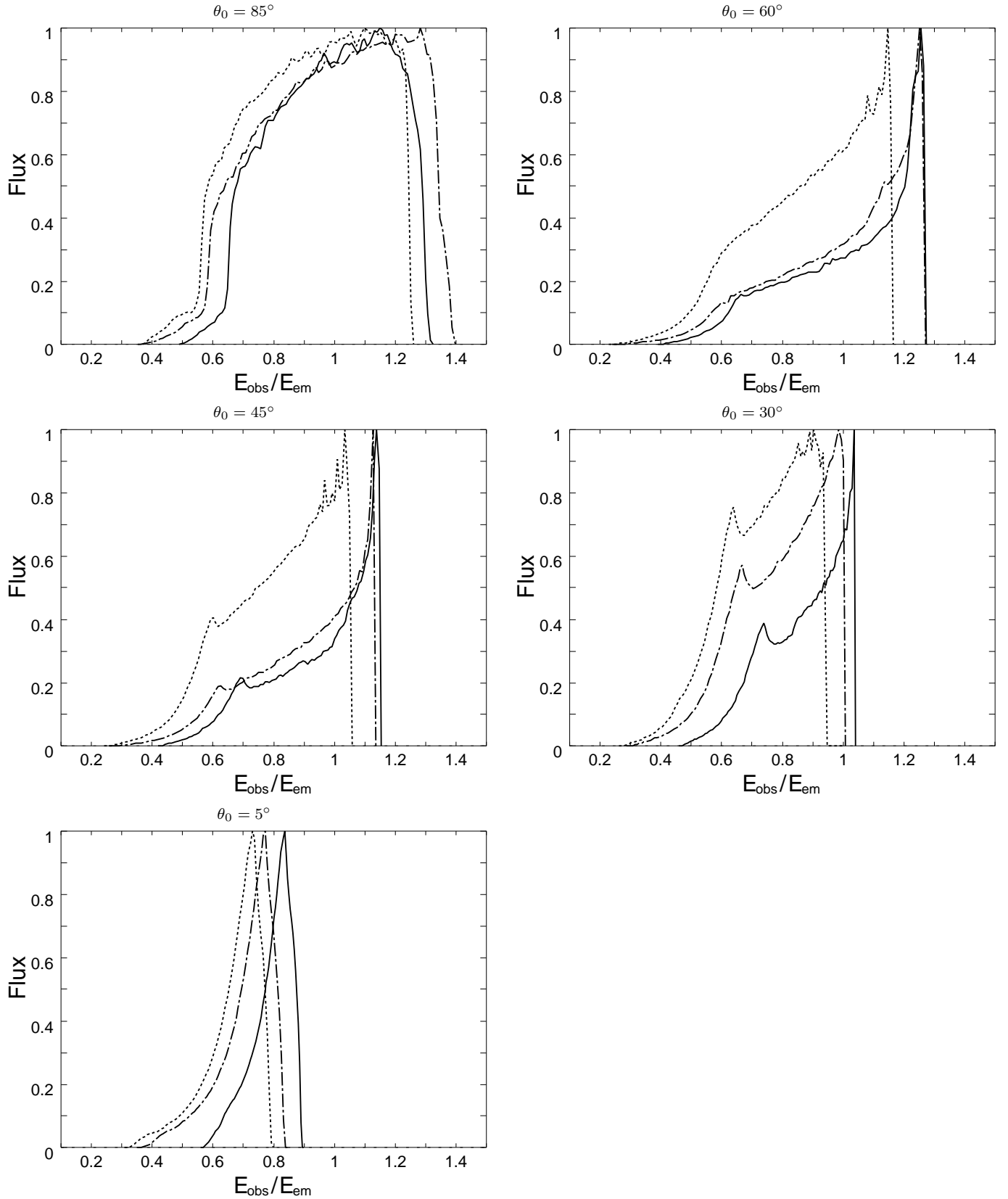


Figure 5. Same as Fig. 4 but for Models A (solid line), B (dash-dotted line) and C (dotted line) with $s = -1$.

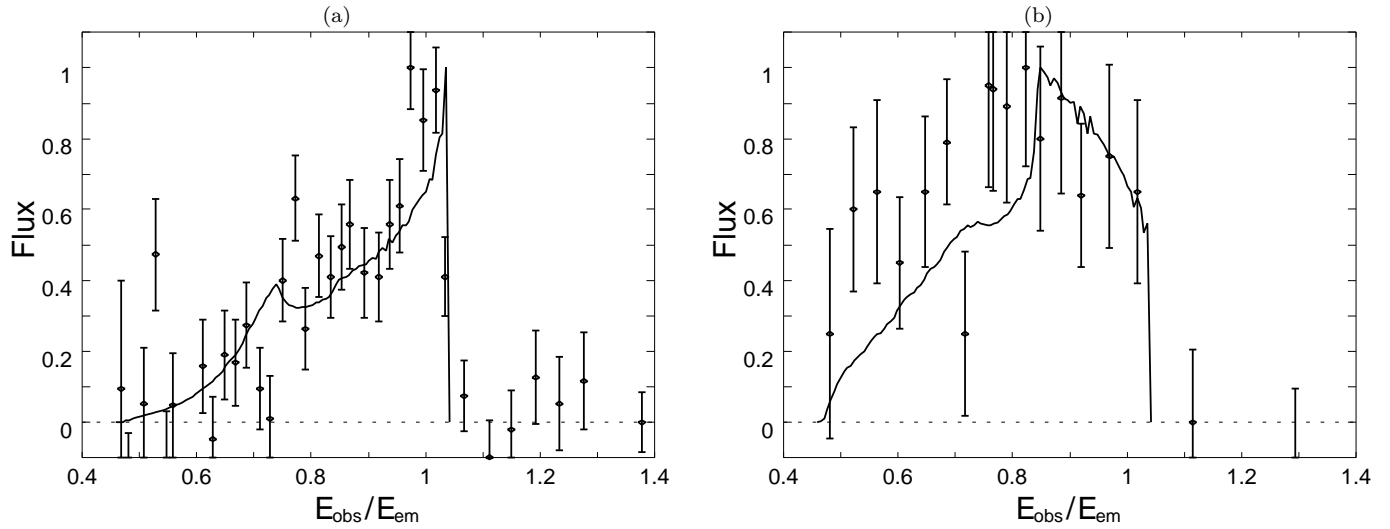


Figure 6. Same as Fig. 4 but for the model with $\theta_0 = 30^\circ$ and emissivity indices (a) $s = -1$ (solid line) and (b) $s = -4$ (solid line). The observational data of the ASCA are plotted by points with error bars for the data of Tanaka et al. (1995) (a) and that of Iwasawa et al. (1996) (b).